

Portland State University

PDXScholar

Dissertations and Theses

Dissertations and Theses

6-1-1968

Precision measurements of the Mössbauer fraction of Fe⁵⁷ in Pt, Pd and Cu

Wilbur Lee Nees

Portland State University

Follow this and additional works at: https://pdxscholar.library.pdx.edu/open_access_etds

Let us know how access to this document benefits you.

Recommended Citation

Nees, Wilbur Lee, "Precision measurements of the Mössbauer fraction of Fe⁵⁷ in Pt, Pd and Cu" (1968). *Dissertations and Theses*. Paper 17.

<https://doi.org/10.15760/etd.17>

This Thesis is brought to you for free and open access. It has been accepted for inclusion in Dissertations and Theses by an authorized administrator of PDXScholar. Please contact us if we can make this document more accessible: pdxscholar@pdx.edu.

AN ABSTRACT OF THE THESIS OF

Wilbur Lee Nees for the Master of Science in Physics

Date thesis is presented May 16, 1968

Title "Precision Measurements of the Mössbauer Fraction of Fe^{57}
in Pt, Pd and Cu"

Abstract approved

Assistant Professor of Physics

Precision measurements of the Mössbauer fraction of the 14.4 keV Fe^{57} transition were made using the black, wide absorber technique. The Fe^{57} was diffused, as a dilute Mössbauer impurity, into 99.995% purity single crystal chips of Pt, Pd and Cu. By comparing the Debye form of $-\ln f$, corrected for anharmonicity, with our data, we extracted a high and low temperature Debye theta, as well as an anharmonicity coefficient, ϵ , for the three materials. We estimated the accuracy of our data to be $\pm 1\%$. From the data we concluded that the Fe^{57} in Cu has stronger force constants and is more anharmonic than pure Cu, while Fe^{57} in Pt and Pd has smaller force constants and about the same anharmonicity as the pure host materials.

PRECISION MEASUREMENTS OF THE MÖSSBAUER FRACTION OF Fe^{57}

IN Pt, Pd AND Cu

by

WILBUR LEE NEES

A THESIS

submitted to

PORTLAND STATE COLLEGE

**in partial fulfillment of
the requirements for the
degree of**

MASTER OF SCIENCE

June 1968

**PORTLAND STATE COLLEGE
LIBRARY**

APPROVED:


Assistant Professor of Physics


**Head of Department
Physics Department**


Dean of Graduate Studies

Date thesis is presented May 16, 1968

ACKNOWLEDGEMENTS

This author wishes to thank the Tektronix Foundation for its fellowship and NSF for its support. My many thanks to my thesis committee, in particular to Professors D. G. Howard, R. H. Nussbaum and D. Wright for their many suggestions, help, and prodding. Last but not least I wish to thank my wife Cheryl, whose patience and enthusiasm helped me through Graduate school.

TABLE OF CONTENTS

	PAGE
I. Introduction	1
II. Theory	6
Zero-phonon Fraction	6
Line Shapes	18
III. Experimental	21
Sample Preparation	21
Line Shape Measurements	23
f-measurements	26
IV. Data Presentation And Analysis	36
V. Bibliography	47

FIGURE	PAGE
1. Decay scheme of Co^{57} to Fe^{57}	4
2. Dispersion relations of the Debye model and the Monatomic Linear Lattice.	4
3. Density of states for Copper and for the Debye model.	13
4. The energy spectrum of Fe^{57} in Pt.	22
5. Block diagram of the equipment used in the line shape measurements.	24
6. Temperature compensated D.C. amplifier.	25
7. Cold finger of the liquid nitrogen cryostat.	27
8. High temperature furnace used in making f-measurements.	28
9. Block diagram of the equipment used in making f-measurements.	30
10. The recoil free fraction of Fe^{57} in a single crystal of Pt.	40
11. The recoil free fraction of Fe^{57} in single crystal Pd.	41
12. The recoil free fraction of Fe^{57} in single crystal Cu.	42
13. The low temperature Pt data versus T^2 .	43
14. The low temperature Pd data versus T^2 .	44

TABLES

I. Summary of Data	45
--------------------	----

Precision Measurements of the Mössbauer Fraction of Fe^{57} in Pt, Pd and Cu

I. Introduction

There is a finite probability that an excited nucleus, which is bound in a crystal lattice, will decay by emitting a γ -ray, but the recoil momentum will not generate a phonon in the lattice. Such an emission of γ -rays which possess full transition energy is called the Mössbauer effect*. The probability of such a zero-phonon process depends on the binding force between the emitting atom and the lattice, on the γ -ray energy and on temperature. In the next section it is shown that the zero-phonon fraction, f , of the emitted γ -rays is a measure of the mean squared displacement, $\langle x^2 \rangle$, of the emitting atom. The value of $\langle x^2 \rangle$ found from the measured values of f can be compared to the value of $\langle x^2 \rangle$ calculated for certain models of harmonic lattices. The differences between experiment and theory give information about the anharmonicity of the forces between the Mössbauer impurity and the atoms in the lattice. Precision f -measurements of a dilute Mössbauer impurity in a pure host lattice also yield information about the binding forces between impurity and host and can be compared to the host-host binding, provided information from other experiments on the pure host materials are available.

This paper proposes to study the force constants and anharmonicities of dilute Fe^{57} diffused into single crystal chips of Pt, Pd and Cu. The Mössbauer effect will be used to measure the interaction of the Fe^{57} with the host materials. By measuring f over a temperature range from liquid helium into a region where classical equipartition of energy will

* For a more thorough discussion of the Mössbauer effect the reader is directed to books by Wertheim¹ and Frauenfelder².

hold, the data can be compared with the high and low temperature limits of the harmonic crystal models. The data must be accurate enough at high temperatures to estimate the effects of anharmonicity, which can not be ignored. This paper will also present the theory of a monatomic linear lattice, show our experimental methods for making f -measurements, and compare our results with the predictions of the theories.

Previous work on Fe^{57} f -measurements has been published by several investigators^{3,4,5,6,7,8} on several different materials. We chose to re-investigate Pt and Pd because some of these previous results indicated an anomalously low zero-phonon fraction at both high and low temperatures. Copper was included in our study because it has been rather thoroughly studied^{3,4,5} and could be used as a standard with which we could compare our results.

The Fe^{57} Mössbauer impurity is supplied as Co^{57} . The Co^{57} decay scheme can be seen in figure 1. The Co^{57} was diffused into high purity single crystals of Pt, Pd and Cu as a dilute Mössbauer impurity. The zero-phonon fraction of Pt and Pd was measured over a temperature range of approximately 10°K to 750°K. The f of Cu was measured above 100°K since previous low temperature data of comparable accuracy are available⁵.

Two primary sets of measurements were made in this experiment. They both use the fact that the 14.4keV γ -ray emitted without energy loss to the lattice has a very narrow energy distribution, 5×10^{-9} eV, and that an absorber containing stable Fe^{57} nuclei will resonantly absorb the zero-phonon radiation. By mounting the source on a speaker drive assembly

and moving it relative to the absorber, the emitted γ -ray will be Doppler shifted in or out of resonance. If the γ -ray is Doppler shifted into resonant absorption, the reduction of the intensity of the 14.4keV radiation transmitted through the absorber can be detected. The resulting intensity versus Doppler velocity is called a Mössbauer spectrum.

Internal conversion occurs when an excited nucleus decays by ejecting an orbital electron rather than a γ -ray. The internal conversion coefficient is defined by $\alpha = \lambda_e/\lambda_\gamma$, where λ_e and λ_γ are the transition probabilities of the competing processes. The internal conversion coefficient, α , for the 14.4keV transition, shown in the Co^{57} decay scheme in figure 1, is 9.7. This value of α predicts that a resonantly absorbing Fe^{57} atom will decay from its 14.4keV excited state by emission of internal conversion electrons about 93% of the time and will re-emit a γ -ray only 7% of the time. The large value of α for the 14.4keV transition will only slightly increase the resonant radiation transmitted by the absorber, thus effectively reducing the measured absorption.

Before each f study, preliminary measurements of the Mössbauer emission line shape were taken using a resonant absorber of known width. These data yield information about the uniformity of the impurity sites in the source. As we are interested only in the iron-host interaction in equivalent substitutional sites, any anomalous broadening of the emission line could make the source useless.

The primary measurements yield the Mössbauer fraction of the 14.4 keV emission line as a function of temperature. Three different experimental configurations were used, each one had different spacings between source and absorber and between absorber and detector. This meant

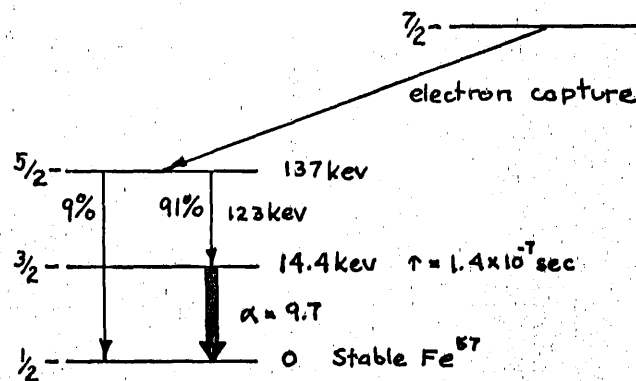


Figure 1. Decay scheme of Co^{57} to Fe^{57} .

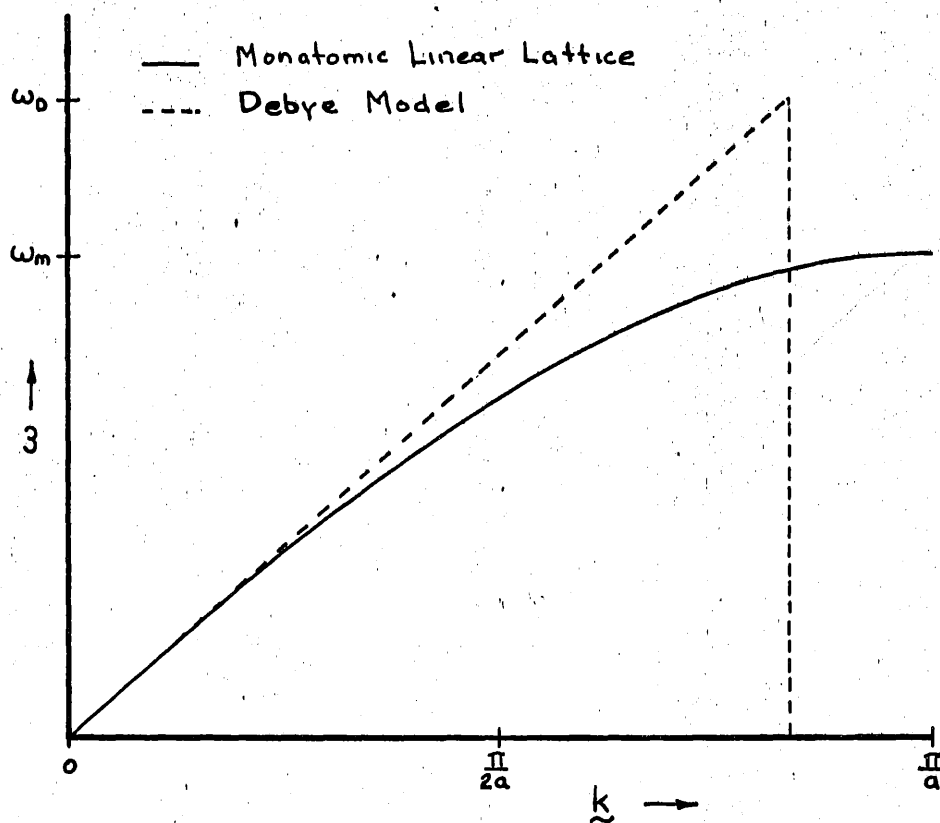


Figure 2. Dispersion relations of the Debye model and the Monatomic Linear Lattice.

that the subtended solid angles and the amount of inelastic scattering of radiation were different for each configuration. A liquid helium cryostat was used for measurements in the range from room temperature down to 10°K . A vacuum furnace was used to heat the source from room temperature to 750°K . A third set of measurements were made at room temperature without interfering radiation windows and at optimum geometrical distances. This last set of measurements served as references to experimentally obtain necessary corrections to the f-measurements made in the cryostat and furnace.

The temperature dependence of f was compared with two different harmonic lattice models. These models, the Debye and the Einstein, are discussed in the theory section of this paper. The experimental corrections and a description of the equipment is given in the experimental section. A final section summarizes the data and some conclusions.

II. Theory

Zero-phonon Fraction

The probability of a transition from a initial nuclear state N_i and lattice state L_i to a final nuclear state N_f and lattice state L_f is given by²:

$$1) \quad W(N_i: N_f, L_i: L_f) = c \left| \langle f | H_{int} | i \rangle \right|^2,$$

where $\langle f |$ and $| i \rangle$ are the final and initial states of the entire system of nucleus, lattice and electromagnetic field. H_{int} is the interaction Hamiltonian. The total probability, normalized to unity, is the sum of W over all possible initial and final lattice and nuclear states. The Mössbauer effect is the nuclear transition N_i to N_f with no simultaneous lattice transition. In this transition, $L_i = L_f$, the γ -ray is emitted recoillessly.

Using the interaction Hamiltonian of a charged particle, moving with momentum p , in an electromagnetic field given by a vector potential A , the probability of a nuclear decay is given by²:

$$2) \quad W(N_i: N_f) = c' \left| \langle f | e^{ik \cdot x} p_A | i \rangle \right|^2$$

if the vector potential is expanded in plane waves. The momentum operator p_A , which is part of the nuclear transition, is in the direction of k , the wavevector of the emitted γ -ray, while x is the coordinate vector of the decaying nucleus.

Because nuclear forces are of extremely short range, compared to the lattice spacing, an approximation can be made that the lattice states do not depend on the nuclear states, hence the nuclear decay is

not influenced by the lattice states and vice versa². Equation 2 can be rewritten² as:

$$3) \quad W = c' |\langle L_f | e^{i\mathbf{k} \cdot \mathbf{x}} | L_i \rangle \langle N \rangle|^2 = c' |\langle L_f | e^{i\mathbf{k} \cdot \mathbf{x}} | L_i \rangle|^2 |\langle N \rangle|^2$$

where $\langle N \rangle$ includes p_A and depends only on the nuclear properties. The recoilless fraction of emitted γ -rays is defined by summing equation 3 over all possible nuclear transitions, with the condition $L_i = L_f$, and dividing by equation 3 summed over all possible lattice and nuclear transitions. Therefore f becomes:

$$4) \quad f = \frac{|\langle L_i | e^{i\mathbf{k} \cdot \mathbf{x}} | L_i \rangle|^2}{\sum_{L_f} |\langle L_f | e^{i\mathbf{k} \cdot \mathbf{x}} | L_i \rangle|^2} = |\langle L_i | e^{i\mathbf{k} \cdot \mathbf{x}} | L_i \rangle|^2$$

where the denominator, the total lattice transition probability, is normalized to one.

Boyle and Hall¹⁰ show that, assuming harmonic forces, equation 4 can be rewritten:

$$5) \quad f = e^{-k^2 \langle x^2 \rangle} = e^{-\langle x^2 \rangle / \lambda^2}$$

$$-\ln f = \langle x^2 \rangle / \lambda^2$$

where λ is the reduced wavelength and $\langle x^2 \rangle$ is the component of the mean squared displacement of the excited nucleus in the direction of the emitted γ -ray. $\langle x^2 \rangle$ is a thermal average of the atomic displacement due to each normal mode of vibration over a time interval equal to the lifetime of the nuclear level responsible for the emission. The quantity $\langle x^2 \rangle / \lambda^2$ corresponds to the well known Debye-Waller factor in x-ray diffraction.

The calculation of $\langle x^2 \rangle$ is basically a lattice dynamics problem.

It is convenient at this point to put $\langle x^2 \rangle$ into a different form. Assuming that the lattice forces are harmonic, the normal modes of vibration of the lattice are independent. By representing the crystal as $3N$ harmonic oscillators ω_j , the average energy of each oscillator can be written as:

$$6) \quad \langle E_j \rangle = \langle n(\omega_j) + \frac{1}{2} \rangle \hbar \omega_j$$

where $n(\omega_j)$ is the phonon occupancy of the mode at frequency ω_j . Hence the energy of the crystal due to the j^{th} oscillator can be related to the mean squared displacement of that oscillator by:

$$7) \quad NM \omega_j^2 \langle x_j^2 \rangle = \langle n(\omega_j) + \frac{1}{2} \rangle \hbar \omega_j$$

The average mean squared displacement of the crystal is found by summing over all the normal modes of the harmonic crystal:

$$8) \quad \langle x^2 \rangle = \frac{\hbar}{NM} \sum_j \frac{\langle n(\omega_j) + \frac{1}{2} \rangle}{\omega_j}$$

N is the number of atoms involved and M is the mass of one atom. If the number of states, j , are assumed close enough together, a continuum can be used to replace the discrete levels. Then the summation in equation 8 can be replaced with an integral:

$$9) \quad \langle x^2 \rangle = \frac{\hbar}{NM} \int_0^\infty \langle n(\omega) + \frac{1}{2} \rangle \frac{D(\omega)}{\omega} d\omega$$

where $D(\omega)$ is defined¹¹ as the number of phonon states per unit frequency range. Assuming an isotropic material we have¹¹:

$$10) \quad D(\omega) = D(k) \frac{dk}{d\omega} 4\pi k^2$$

where $dk/d\omega$, the group velocity, is the first derivative of the dispersion relation. $D(k)$, the density of states in k -space, is the number of modes per unit range in k , which is determined from the boundary conditions of the crystal. If the crystal is in thermal equilibrium, the phonon occupancy can be given by a Bose-Einstein distribution and equation 9 becomes:

$$11) \quad \langle x^2 \rangle = \frac{\hbar^2}{NM} \int_0^\infty \left[\frac{1}{2} + \frac{1}{e^{\hbar\omega/kT} - 1} \right] \frac{D(\omega)}{\omega} d\omega$$

Now the mean squared displacement is clearly temperature dependent.

In order to evaluate equation 11 for $\langle x^2 \rangle$, $D(\omega)$ must be known. This is generally a very difficult problem, hence some convenient model for the crystal must be substituted. Some insight into this problem can be gained by considering first a monatomic linear lattice. This lattice is composed of parallel planes, N by N atoms per plane. In the linear lattice all the atoms are fixed in these planes, which are constrained to move in one direction perpendicular to the planes. With the previous assumptions, the general equation of motion for the atomic planes is:

$$12) \quad N^2 M \ddot{u}_n = \sum_{j \neq 0} F_{n,n+j} (u_{n+j} - u_n)$$

u_n is the displacement of the atoms in the n -th plane from their equilibrium positions, \ddot{u}_n is the second time derivative, M the mass of the atom, and $F_{n,n+j}$ the total force between planes n and $n+j$. Dividing through by $N^2 M$ and setting $n=0$, using $+j$ for planes on one side of the $n=0$ plane and $-j$ for those on the other side:

$$13) \quad \ddot{u}_0 = \frac{1}{M} \sum_{j=1}^{\infty} \frac{F_j}{N^2} (u_j + u_{-j} - 2u_0) = \frac{1}{M} \sum_{j=1}^{\infty} f_j (u_j + u_{-j} - 2u_0)$$

The solution to equation 13 is a longitudinal traveling wave. This formalism is equally good for both transverse and longitudinal waves.

If only nearest neighbor interactions are considered, i.e. $f_j=0$ for $|j| > 1$, then a traveling wave of the form¹¹:

$$14) \quad u_j = u(0) e^{i(jka - \omega t)}$$

is obtained, where a is the lattice spacing; k is the wavenumber; and ω is the normal mode frequency. Substituting the solution (14) in equation 13 yields a dispersion relation:

$$15) \quad \omega = \sqrt{\frac{4f}{M}} \left| \sin \frac{ka}{2} \right| = \omega_m \left| \sin \frac{ka}{2} \right|$$

When $k = \frac{\pi}{a}$, ω is a maximum value ω_m , called the cutoff frequency of the lattice. In other words there is a maximum frequency which can propagate through a crystal lattice. When the normal modes are assumed to be quantized, they are called phonons, each having an energy $\hbar\omega$.

The density of states for the monotomic linear lattice is found by taking the derivative of ω with respect to k in equation 15, then substituting the result into equation 10, which yields:

$$16) \quad D(\omega) = \frac{4V}{\pi^2 a^3} \frac{\left[\sin^{-1} \left(\frac{\omega}{\omega_m} \right) \right]^2}{\sqrt{\omega_m^2 - \omega^2}}$$

where V is the lattice volume and a the lattice spacing. Because of the complex form of $D(\omega)$, it is very difficult to evaluate equation 11, although it has been done by Visscher¹². Usually an approximation is made to facilitate the solution for $\langle x^2 \rangle$.

The approximation considered first will be the Debye approximation. The dispersion relation for the Debye model is given by¹¹:

$$\begin{aligned}
 17) \quad \omega &= v k & k &\leq k_m \\
 \omega &= 0 & k &> k_m
 \end{aligned}$$

such that $v = \lim_{k \rightarrow 0} \frac{d\omega}{dk}$ for the real lattice. This dispersion relation says that v , the velocity of propagation of sound in the lattice, is a constant. Equation 17, the Debye approximation, is compared with equation 15, the monatomic lattice, in figure 2. The dispersion relation is arbitrarily cutoff at ω_D at the limit k_m . The Debye cutoff frequency, ω_D , can be related to a characteristic temperature, θ_D , by an energy relation:

$$18) \quad \hbar \omega_D = k \theta_D$$

This Debye theta is used as a suitable parameter for comparison of thermal and elastic properties of materials from different types of measurements.

The density of states is normalized so the total number of states in the model will equal the total number of vibrational modes in the crystal, which is $3N$, that is:

$$19) \quad \int_0^{\infty} D(\omega) d\omega = 3N$$

If the Debye model is normalized using equation 19 the upper limit of the integral is set to ω_D to keep the left hand side of the equation from diverging when the Debye density of states, $D(\omega) = \omega^2$ is used. After normalization, the Debye $D(\omega)$ becomes^{1,11}:

$$20) \quad D(\omega) = 9N \frac{\omega^2}{\omega_D^3}$$

which defines ω_D , the Debye cutoff frequency. N is the total number of atoms. The real density of states for Cu, as obtained from neutron scattering experiments by Nicklow, et. al.¹³, is compared, in figure 3, with a Debye density of states for the equivalent Debye theta.

Substituting equation 20 into equation 11 yields an expression¹ for $\langle x^2 \rangle$:

$$21) \quad \langle x^2 \rangle = \frac{3}{4} \frac{\hbar^2}{Mk\Theta_D} \left[1 + 4 \left(\frac{T}{\Theta_D} \right)^2 \int_0^{\Theta_D/T} \frac{u du}{e^u - 1} \right]$$

then substituting equation 21 into the expression for f , equation 5:

$$22) \quad -\ln f_D = \frac{3}{4} \frac{\hbar^2}{Mk\Theta_D \lambda^2} \left[1 + 4 \left(\frac{T}{\Theta_D} \right)^2 \int_0^{\Theta_D/T} \frac{u du}{e^u - 1} \right]$$

This integral form for the Debye model has been tabulated by A.H. Muir¹⁴.

Two useful limiting forms for $-\ln f$ can be shown to follow from equation 22. The first is the high temperature limit, $T \gg \Theta_D$ or $u \ll 1$.

Expanding e^u in equation 22, the integral becomes:

$$23) \quad \int_0^{\Theta_D/T} \frac{u du}{e^u - 1} = \int_0^{\Theta_D/T} \frac{u du}{(1 - u + u^2/2 - \dots)} \approx \frac{\Theta_D}{T} \quad : \text{for } T \gg \Theta_D$$

then equation 22 becomes:

$$24) \quad -\ln f_D = \frac{3}{4} \frac{\hbar^2}{Mk\Theta_D \lambda^2} \left[1 + 4 \frac{T}{\Theta_D} \right] \approx \frac{3}{2} R \frac{T}{K\Theta_D^2}$$

where $R = \frac{\hbar^2}{2M\lambda^2} = \frac{E_r^2}{2Mc^2}$ is the recoil energy.

At the low temperature limit, $T \ll \Theta_D$, the upper limit of the integral in equation 23 is essentially ∞ , and the integral can be evaluated exactly:

$$25) \quad \int_0^{\infty} \frac{u du}{e^u - 1} = \frac{\pi^2}{6}$$

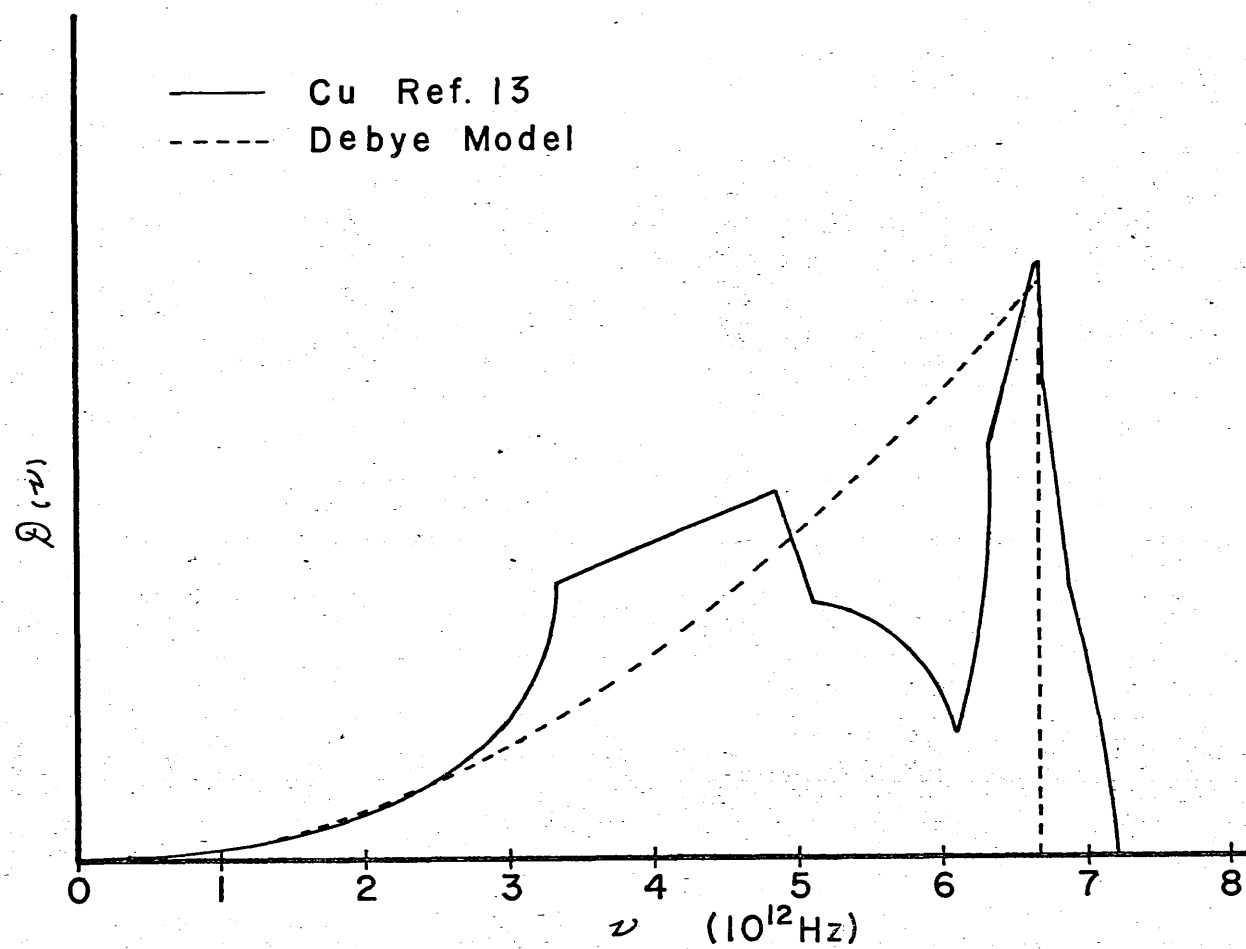


Figure 3. Density of states for Copper and for the Debye model.

so in the low temperature limit, $-\ln f$ is given by:

$$26) \quad -\ln f_D \approx \frac{6R}{4k\theta_D} \left[1 + \frac{2}{3} \left(\frac{\pi T}{\theta_D} \right)^2 \right] = \frac{R}{k\theta_D} \left[\frac{3}{2} + \frac{\pi^2 T^2}{\theta_D^2} \right]$$

So far, the forces present in the crystal have been assumed to be harmonic, while in fact all crystals have some inherent anharmonicity. The coefficient of linear expansion results from the anharmonicity of the crystal potential. If a classical approach is used and the crystal potential is no longer assumed harmonic, the potential takes the form:

$$27) \quad V = V_0 + s x^2 + g x^3 + h x^4 + l x^5 + \dots$$

The mean squared displacement for a Boltzman distribution is:

$$28) \quad \langle x^2 \rangle = \frac{\int_{-\infty}^{\infty} x^2 e^{-\beta E(x)} dx}{\int_{-\infty}^{\infty} e^{-\beta E(x)} dx}$$

where $\beta = \frac{1}{kT}$ and $E(x) = V(x) + \text{K.E.}$ The kinetic energy terms cancel in the above equation leaving:

$$29) \quad \langle x^2 \rangle = \frac{\int_{-\infty}^{\infty} x^2 e^{-\beta V(x)} dx}{\int_{-\infty}^{\infty} e^{-\beta V(x)} dx}$$

Substituting in the potential energy expression and making the assumption that only the cubic and quartic terms of the potential add significantly to the harmonic potential, equation 29 becomes:

$$30) \quad \langle x^2 \rangle = \frac{\int_{-\infty}^{\infty} x^2 e^{-\beta s x^2} dx - \beta h \int_{-\infty}^{\infty} x^4 e^{-\beta s x^2} dx}{\frac{1}{2} \left(1 - \frac{h}{s^2} kT - \dots \right)}$$

which integrates to:

$$31) \quad \langle x^2 \rangle = \frac{1}{2s} kT - \frac{3}{2} \frac{h}{s^3} (kT)^2 + \dots$$

If s is defined by:

$$32) \quad s = \frac{1}{2} \left(\frac{d^2V}{dr^2} \right)_{r_0(T)} \quad \text{and} \quad \frac{\partial s}{\partial T} = \frac{1}{2} \left(\frac{d^3V}{dr^3} \right)_{r_0(T)} \frac{dr}{dT} = 3g\alpha$$

at temperature T and $\alpha = \frac{dr}{dT}$ is the coefficient of linear expansion.

s can be expanded to:

$$33) \quad s = s_0(1 + 3\alpha gT + \dots)$$

Substituting equation 33 into 31 yields:

$$34) \quad \langle x^2 \rangle = \frac{1}{2s_0} kT - \frac{3}{2} \left(\frac{g\alpha}{s_0 k} + \frac{h}{s_0^3} \right) (kT)^2 \quad ; \text{ to order } T^2$$

Then defining ϵ as:

$$35) \quad \epsilon = \left(3g\alpha + \frac{3h}{s_0^2} \right) k$$

allows equation 34 to be put in the following form:

$$36) \quad \langle x^2 \rangle \simeq \frac{kT}{2s_0} (1 + \epsilon T)$$

A quantum mechanical calculation by Maradudin and Flinn¹⁵ who introduced small cubic and quartic anharmonic terms to a harmonic crystal force model, obtained in the high temperature limit:

$$37) \quad -\ln f = -\ln f_H (1 + \epsilon T)$$

where f_H is the harmonic Mössbauer fraction and ϵ is an anharmonicity term depending on the derivatives of the potential function¹⁵. If equation 36 is inserted into $-\ln f$, equation 5, the resulting expression agrees with the Maradudin and Flinn result, equation 37.

We made the assumption that we may use one value of the anharmonicity correction over the full temperature range of our measurements.

Using the Debye expression for $-\ln f$, equation 22, for the harmonic Mössbauer fraction, equation 37 yields f as a function of temperature:

$$38) \quad -\ln f = -\ln f_D (1 + \epsilon T)$$

This expression fits our data very well, as can be seen in figures 10 through 12.

It must be remembered that the Debye model treats the Mössbauer atom as identical to the host lattice, not as a dilute impurity. It might be expected that Fe^{57} will act differently than a host atom at the same site. Thus perhaps a different $D(\omega)$ might be expected. In order to understand the nature of the change in $D(\omega)$, we return to the linear monatomic lattice, now with a light impurity replacing one of the regular atoms. In this model the light impurity atom is pictured rattling around in a box made of the more massive host atoms, but with no change in the interatomic force constant f . The light atom can respond to higher frequencies than the heavier host; therefore, there would be an extra solution to the equation of motion, corresponding to a spatially damped wave centered at the impurity sites.

The equations of motion for the monatomic linear lattice with a light impurity, $M' < M$, assuming harmonic forces and nearest neighbor interactions only, are:

$$39) \quad M \ddot{u}_j = f(u_{j+1} + u_{j-1} - 2u_j) \quad j \neq 0$$

$$40) \quad M' \ddot{u}_0 = f(u_1 + u_{-1} - 2u_0)$$

Between the Brillouin zone boundaries the solutions are still traveling waves as before, but at the zone boundaries, because of the mass differ-

ence, there will be a solution at the impurity site' that is not coupled to the lattice. This solution must approach the regular standing wave solution as M' approached M . One form of this solution is given by¹¹:

$$41) \quad u_j = u(0) (-1)^j e^{i\omega t} e^{-|j|\alpha}$$

where α is the spatial damping factor. When equation 41 is substituted into equations 39 and 40 a pair of simultaneous equations in α and ω result. Solving these equations for ω yields¹¹:

$$42) \quad \omega^2 = \omega_m^2 \left[\frac{M^2}{2MM' - M'^2} \right]$$

The effect of the light mass is to generate a localized vibration mode above the regular phonon spectrum, which is not coupled to the other normal modes. The impurity atom, therefore, partakes in the motion of the lattice through its coupling to the heavier neighbors and it vibrates in a localized mode.

The Einstein approximation considers all atoms as independent harmonic oscillators of a single frequency, ω_E . This approximation can be used to describe the localized vibration mode in the linear lattice. With the single frequency represented by a delta function, the normalized density of states for a monatomic Einstein lattice becomes¹:

$$43) \quad D(\omega) = 3N \delta(\omega - \omega_E)$$

Integrating equation 11 for $\langle x^2 \rangle$ and putting the resulting answer into the expression for $-\ln f$, equation 5:

$$44) \quad -\ln f = \frac{R}{k\theta_E} \left[\frac{1}{2} + \frac{1}{e^{\theta_E/T} - 1} \right]$$

θ_E is defined as before by $\hbar\omega_E = k\theta_E$.

Line Shapes

Before the f-measurements can be interpreted, we must know whether all the decaying atoms occupy the same type of lattice site. Each different site leads to a different isomer shift¹ in the velocity spectrum. The term isomer shift refers to changes in the s-electron density at the position of the nucleus, which causes an altered Coulombic interaction. The altered interaction causes slight shifts in the nuclear levels in different sites. These shifts in nuclear levels result in a slightly different transition energy which we measure as a shift in the position of the velocity spectrum. It is necessary for meaningful f-measurements to have only one Mössbauer site, which yields a well resolved line spectrum. For our measurements we wanted the decaying atoms to be surrounded by and to interact only with the host atoms. Other impurities in the lattice will interact with the Fe^{57} , causing a change in f as well as causing an isomer shift.

The Mössbauer line-shape measurements from one type of site in the lattice will be Lorentzian in shape and have a "natural" full width at half maximum of Γ_L . If more than one type of lattice sites are present or if there are interactions between impurities, the energy line will become partially split, lose its Lorentzian shape and/or become widened, $\Gamma_L > \Gamma_L$. The Lorentzian shape of the curve comes from the Fourier transform of the probability distribution of the time of emission of the γ -ray after the creation of the excited state¹⁶. Wertheim¹ has shown that by folding the emission and absorption lines, the resulting line is nearly Lorentzian in shape, and that the composite line width at half

maximum is just the sum of the emission and absorption line widths, if both are natural. That is:

$$45) \quad \Gamma = 2\Gamma_L$$

where Γ_L is the line width for the emitted gamma-ray. Γ_L is given by the uncertainty relation:

$$46) \quad \tau \Gamma_L = \hbar$$

where Γ_L is in energy units and τ is the mean life time of the decaying atom. So far it has been assumed that both the emission and absorption spectra are single lines, but in reality either or both can be quadrupole and/or magnetically split due to internal electric or magnetic fields. In the natural iron absorber used for line shape measurements, the spectrum is magnetically split into six completely resolved lines of natural width due to the nuclear Zeeman effect. We used the two inner lines for our measurements.

The line shapes are taken with the sources mounted on the speaker assembly. A sinusoidal driving voltage is applied to the speakers. The measured absorption spectrum is a function of the relative velocity. The total velocity range is divided into 256 segments in a multichannel analyzer. The measured γ -ray pulses are stored in the segment that corresponds to the instantaneous relative velocity at the instant of emission. If the driving velocity changed linearly from positive to negative velocity, randomly generated pulses would be stored with equal probability in all 256 velocity channels. Because of the sinusoidal driving velocity, the source spends more time at higher velocities than at lower veloc-

ities. This unequal dwell-time results in an inherent bias in favor of the γ -rays emitted at high source velocities. To remove this bias two sets of measurements are made simultaneously. The first set is the 14.4 keV Mössbauer spectrum and the second set is from non-resonant γ -rays, in our case from the high energy radiation from the same source. The non-resonant velocity spectrum is a measure of the time spent in each velocity segment. By dividing the appropriate absolute count in the Mössbauer segment of the analyzer by its non-resonant counter part, the quotient is proportional to the true Mössbauer pulse rate, corrected for channel dwell-time. This process is called normalization. Plotting the count rate as a function of velocity results in an emission line or lines which can then be fitted to a Lorentzian and Γ , in mm/sec, measured.

III. Experimental

Sample Preparation

The Mössbauer sources of Pt, Pd and Cu were cut into small disks about 1/8 to 1/4 of an inch in diameter from 99.995% purity single crystal chips. The sample surfaces were very carefully degreased with trichloroethylene, etched clean with acid, rinsed with distilled water and dried with a cotton swab. The cleaned surfaces were moistened with beef albumen as a wetting agent, onto which was pipetted approximately 1/3 mCi of high specific activity $\text{Co}^{57}\text{Cl}_2$ in HCl.

The sources were then individually heated to 500°C in a H_2 atmosphere, which reduced the CoCl_2 to metallic Co. The system was flushed with He and pumped to a vacuum of better than 10^{-4} Torr. The metallic Co was then diffused into the sources by raising the system temperature to 1000°C for 20 minutes for the Pt and Pd, and to 900°C for 45 minutes for the Cu. The diffusion times and temperatures were chosen after considering the solubility of iron in Pt, Pd and Cu and the melting points of the host materials. The surface activity was removed by scrubbing the source with pumice soap and water.

A γ -ray spectrum was taken of each source, using a Xe- CH_4 filled proportional counter, a FET preamplifier and a 512 channel pulse height analyzer. The Pd and Cu sources showed a well resolved 14.4keV peak, but the Pt source had one of the L x-rays included within the 14.4keV peak, as shown in figure 4. From relative intensities of the other Pt L x-ray peaks¹⁷ and from some measurements made for us by V.O. Kostroun using a calibrated Si(Li) spectrometer at the University of Oregon, we estimate that this L x-ray contributes about 1% to the 14.4keV peak.

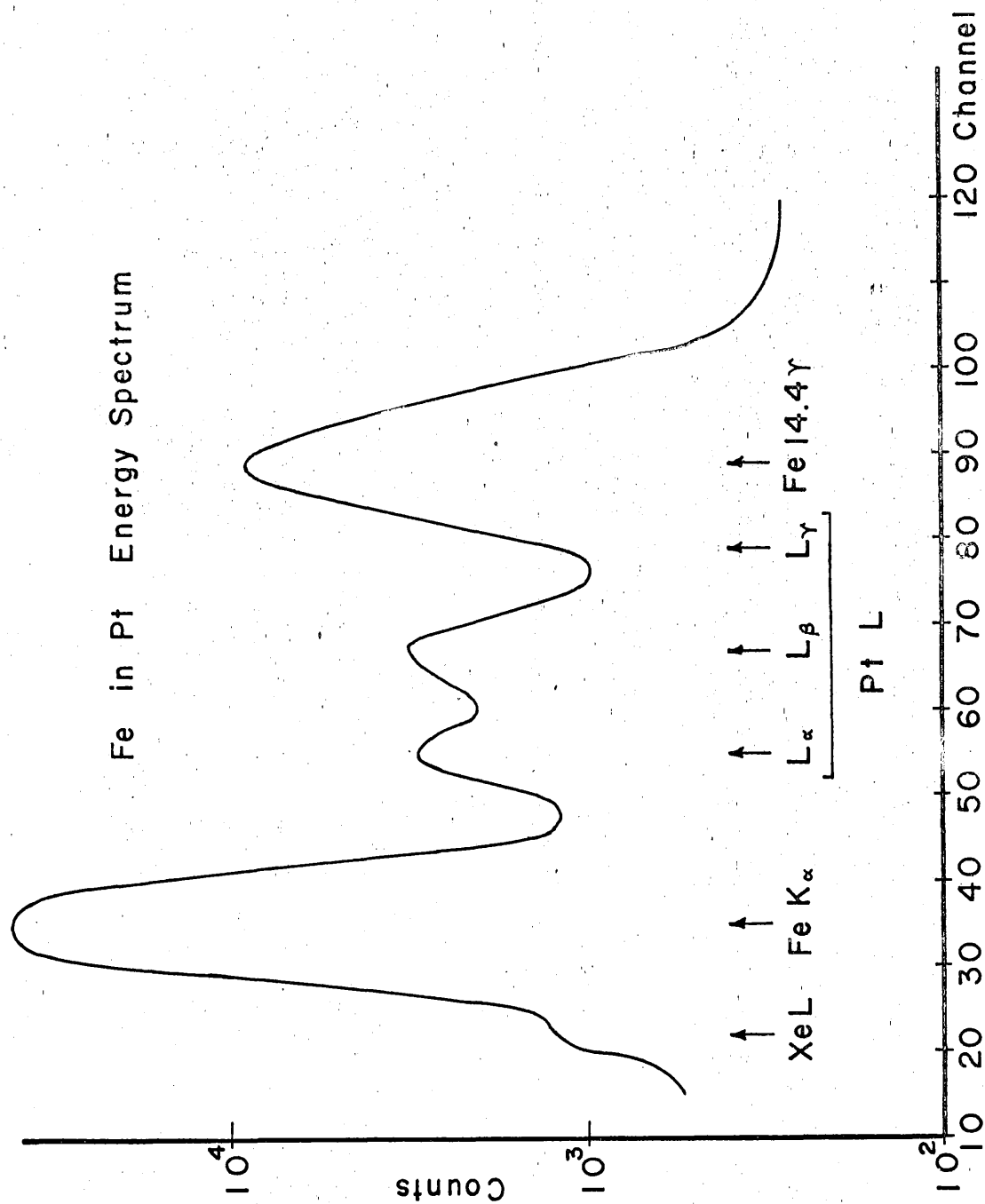


Figure 4. The energy spectrum of ^{57}Fe in Pt.

Line Shape Measurements

To measure the line shapes, the sources were mounted on a double speaker drive assembly, which was driven at approximately 20Hz. The block diagram for these measurements is given in figure 5. A natural iron absorber was placed between the source and the Xe-CH_4 proportional counter. The output was fed to a FET preamplifier, a main amplifier and to two differential pulse height analyzers (DPHA). One of the DPHA's was set on the 14.4keV line and the other, set at an arbitrary higher energy, was used as the normalizing channel. These two sets of signals, which act as trigger signals were fed to a special mixer-router assembly. The mixer-router generates the appropriate set and coincident pulses for the multichannel analyzer, so that the two different trigger signals gate the correct half of the analyzer memory. At the same time that the set and coincident pulses are fed to the analyzer, the 20Hz sine wave is fed from the speaker drive assembly through a temperature compensated D.C. amplifier. Figure 6 gives the electrical schematic of this amplifier. From the D.C. amplifier the sine wave is fed as an analog signal to the analog-to-digital converter (ADC) input of the multichannel analyzer and is sampled whenever a normalizing or 14.4keV trigger signal is present at the coincident input. The trigger signal is stored as a count in a channel corresponding to the instantaneous D.C. voltage at the ADC input which is proportional to the relative velocity of the speaker drive. The total number of events in the analyzer memory is then normalized and plotted as a function of velocity, from which the line shape and width can be obtained.

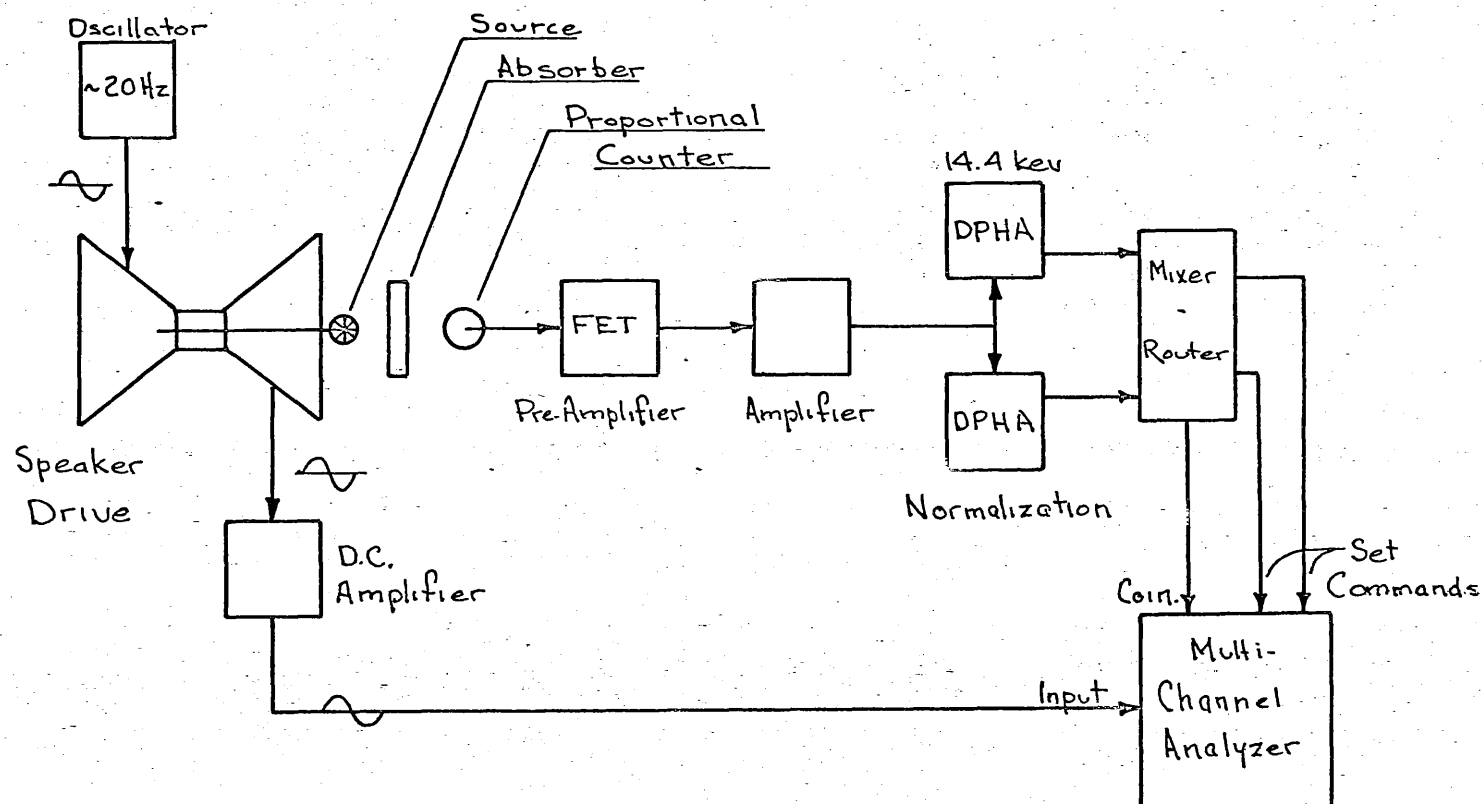


Figure 5. Block diagram of the equipment used in the line shape measurements.

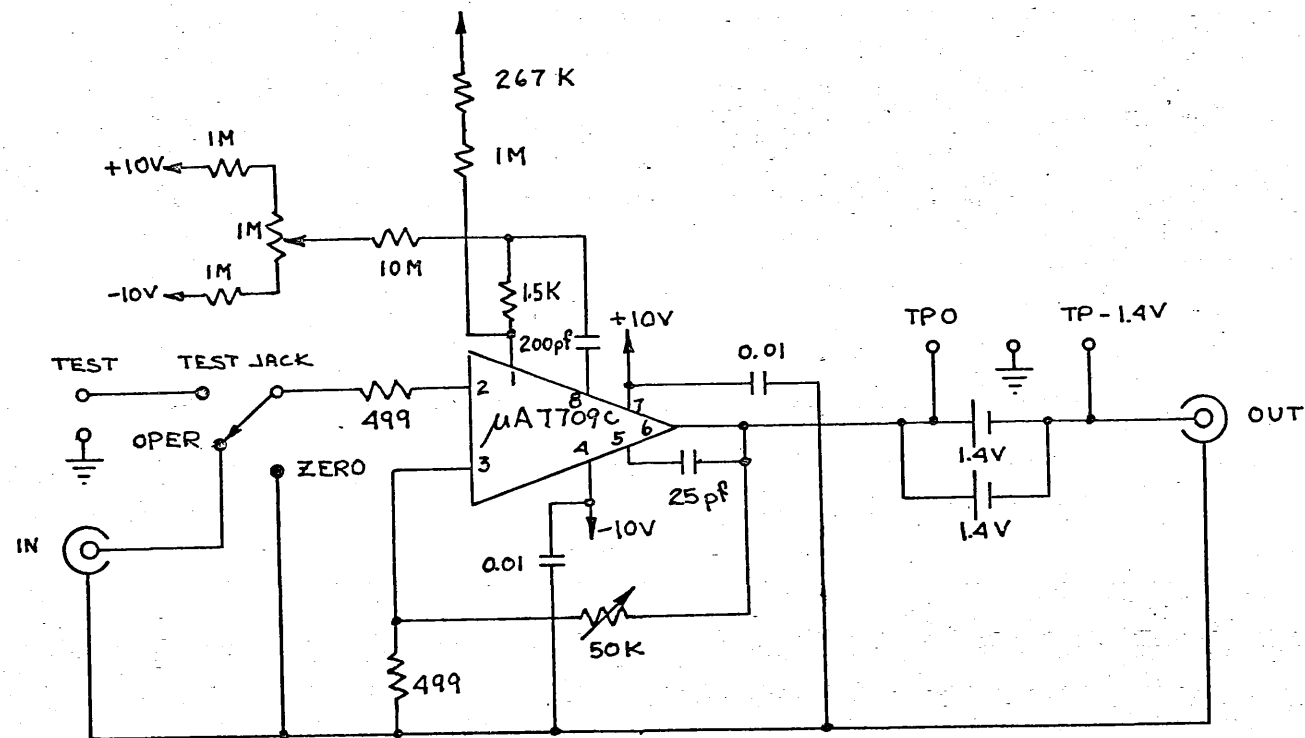


Figure 6. Temperature compensated D.C. amplifier.

f-measurements

We measured the zero-phonon fraction experimentally by the wide, black absorber technique^{3,8}. This method uses an absorber which is much wider at half maximum than the resonant line and which is as nearly opaque (black) to the resonant radiation as is practical. The black absorber technique, with the proper corrections¹⁹, allows absolute f-measurements as a function of temperature.

The complete set of f-measurements required three different experimental arrangements: a low temperature cryostat shown in figure 7, a high temperature furnace shown in figure 8, and a room temperature measurement free of interfering radiation windows and set at optimum geometry. In the third arrangement the sources were mounted on the speaker drive assembly, as shown in figure 9. For the low and high temperature measurements the sources were mounted inside the cryostat or furnace and the absorber was mounted on the speaker drive assembly.

In the furnace, figure 8, a brass plate, with electrical feed-throughs, supports a ceramic rod. The aluminum heat shield is supported by the rod, and the anodized aluminum sample holder is screwed to the end of the rod. Wound around the sample holder is the heater element. A chromel-alumel thermocouple is used to measure the source temperature. The source is held in place against the sample holder by an aluminum spacer and a Be radiation window. The Al heat shield is 1 mil thick in front of the source. The entire assembly is covered with a brass can with an axially mounted Be radiation window.

The cold finger of the nitrogen cryostat, figure 7, consists of an aluminum sample holder with the sample held in by double backed press-

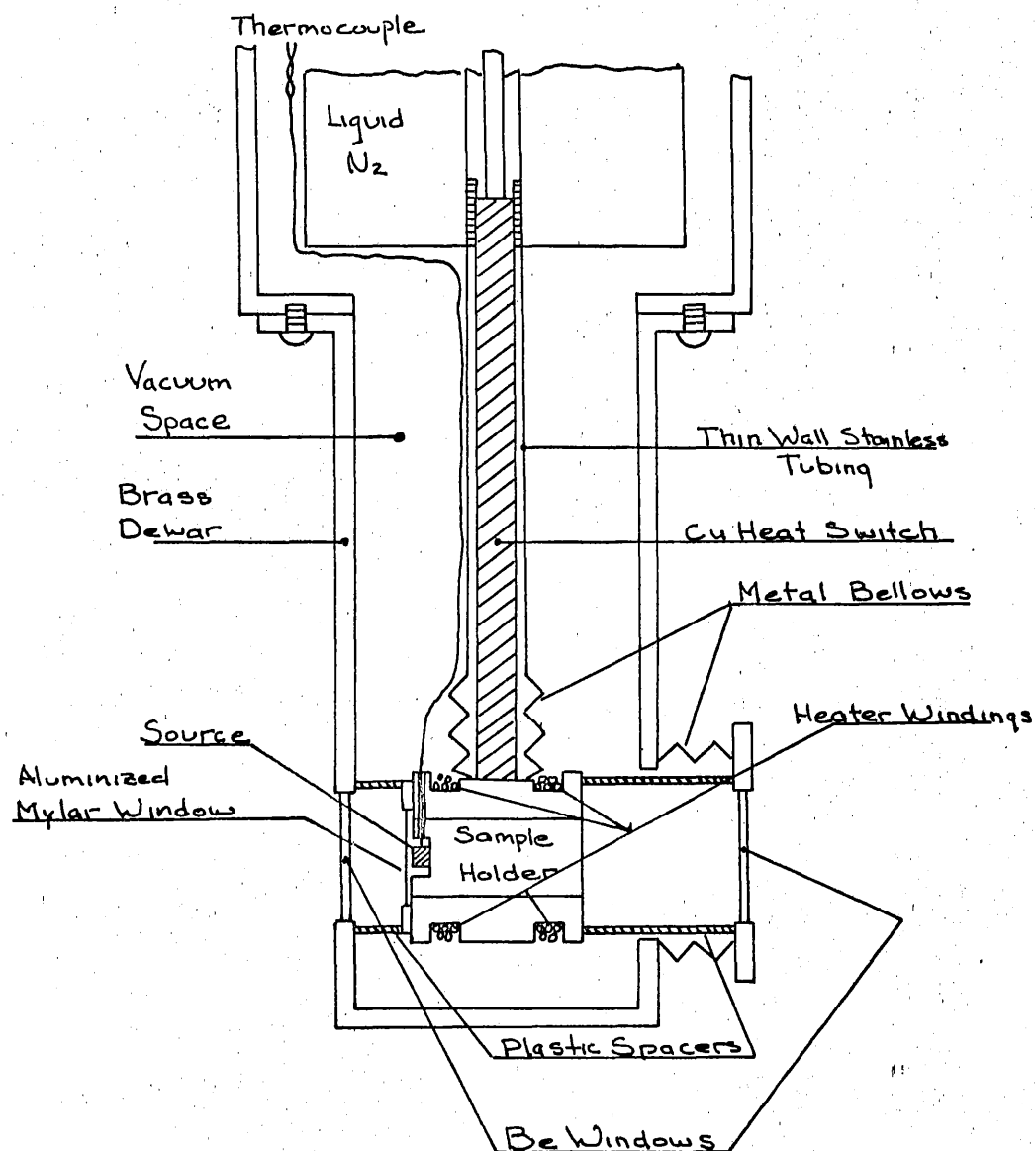


Figure 7. Cold finger of the liquid nitrogen cryostat.

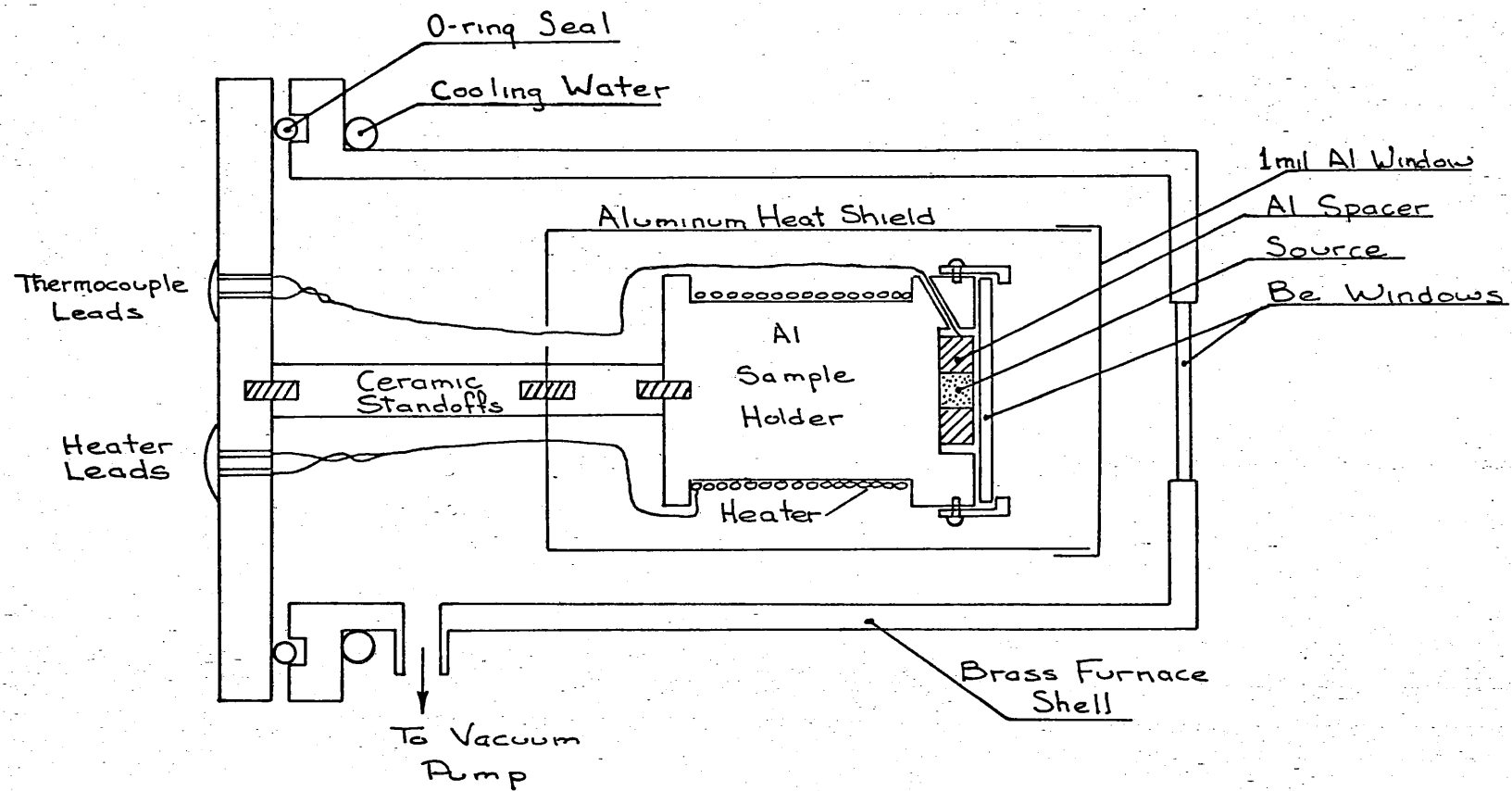


Figure 8. High temperature furnace used in making f-measurements.

ure-sensitive tape and by an aluminized mylar window. The sample holder was supported by a metal bellows and a piece of thinwall stainless steel tubing. The stainless steel acts as an insulator to isolate the source from the low temperature reservoir. A sliding copper rod, acting as a heat switch, in contact with the reservoir, is used to short out the thermal insulator and cool the sample. Wound around the sample holder is the heater winding which when used in conjunction with the heat switch allowed easier temperature stabilization than was possible with the switch alone. A chromel-alumel thermocouple was used to measure the temperature down to 50°K . A second cryostat was used at the University of Washington to approach liquid helium temperatures. The two cryostats were of similar construction except for an additional reservoir and heat shield on the helium cryostat. To measure temperatures below 50°K , a composition resistor was used, in contact with the sample holder, and measured on a low power A.C. bridge. The sample holder was held rigid by two plastic spacers. The entire cold finger was covered by a brass can with two Be radiation windows, one mounted on a metal bellows to clamp the plastic spacers.

The same electronics were used in all three experimental configurations. The block diagram for the room temperature measurement is given in figure 9. The black absorber was placed between the source and the Xe-CH_4 proportional counter. The output from the counter was fed to a FET preamplifier, an amplifier, then to a DPHA set on the 14.4kev peak. The DPHA output was fed to a single channel scalar.

Three separate counts were made at each temperature for a single value of f . The first count, made at zero relative velocity between the

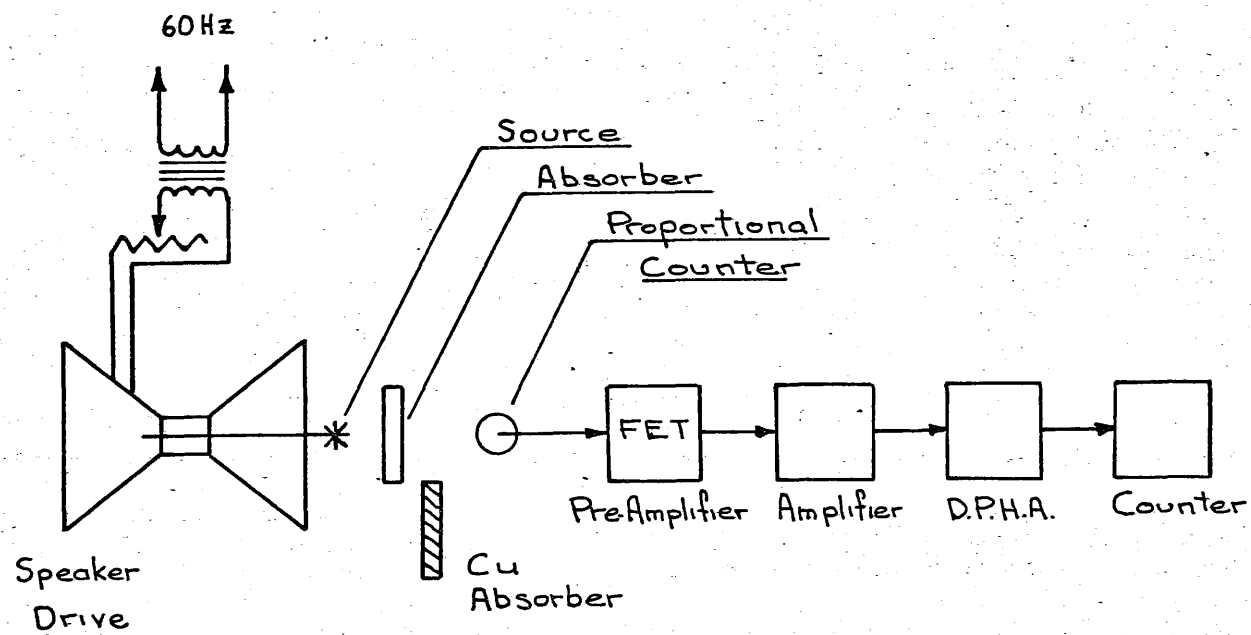


Figure 9. Block diagram of the equipment used in making f-measurements.

wide absorber and the source, is I_o , the total 14.4keV intensity except for the zero-phonon γ -rays. The second count is I_∞ , the total 14.4keV intensity measured with the emission or absorption energy shifted far off resonance. The large energy shift is achieved by driving the speaker with large amplitude 60 Hz sine wave. The third count is also taken far off resonance, but with a copper foil, as a mass absorption filter, inserted between the source and resonant absorber. The copper foil is 99.6 % opaque to the 14.4keV radiation and transmits 98% of the 122keV γ -rays from Fe^{57} . The 122keV radiation plus a few high energy x-rays are responsible for the high energy background. With the copper foil in place, the high energy background, I_B , can be measured because of the elimination of the transmitted low energy radiation. I_B raises the overall count rate in the 14.4keV energy region, since radiation in the high energy range tends to lose only a part of its energy, in the detector.

The experimental f is then given by:

$$47) \quad f = \left[\frac{\beta I_\infty - I_o}{\beta I_\infty - \delta I_B} \right] \frac{1}{C_B} \frac{1}{C_g} \frac{1}{C_c} \frac{1}{C_w}$$

The meaning of the constants is given below:

- β : corrects for the fact that while we were driving the speaker assembly with a large amplitude 60 Hz signal, the relative velocity changed from positive to negative values, passing through zero velocity (resonant absorption). Therefore during the I_∞ measurement, the emission and absorption lines spend a short time in resonance. β was found by plotting I_∞ versus the reciprocal of the speaker driving amplitude. We found β to be 1.008.
- δ : is a correction of 1.02 due to the copper foil absorber trans-

mitting 0.4% of the 14.4keV and only 98% of the 122keV radiation from Fe^{57} .

1- C_B : is a correction for the 3% transmission of the zero-phonon 14.4keV γ -rays through the black absorber. Transmission through the center of the wide line was determined by using a second similar absorber and measuring the increase in the f value. An additional part of the correction is due to the long tail of the emission line falling outside of the opaque region of the absorber. Sprague⁵ calculated the transmission through the wings of the non-Lorentzian absorber to be 2.5%, assuming that the emission spectrum is Lorentzian (supported by our line shape measurements), and using a simplified shape for the absorption wings.

1- C_g : is a correction for the re-radiation of resonant γ -rays from the absorber into the detector. These Mössbauer γ -rays are transmitted through the absorber by two methods. The absorbing atoms re-radiate resonant γ -rays which are then counted as if they had originated in the source. Some of the resonant γ -rays will be Compton scattered, by the electrons in the absorber, out of resonance. This scattered radiation will be counted as non-resonant 14.4keV radiation, and it must be compensated for. The effect is to increase both I_∞ and I_0 by an equal amount. The effect is cancelled in the numerator of equation 47 by subtracting $I_\infty - I_0$. The increase in I_∞ which is also in the denominator then decreases the measured f . An article by Housely¹⁹ shows that C_g depends on the solid angles subtended by the

detector at the absorber, the absorber at the source and the detector at the source, as well as the internal conversion coefficient and the total Compton cross-section for the absorber. The correction for our experiments ranged from 0.2% to 0.8%, depending on the geometry.

$1-C_c$: is the correction for Compton scattering of the Mössbauer γ -rays in the source, as discussed by Housely¹⁹. This correction includes an upper bound for the thermal diffuse scattering. Thermal diffuse scattering of the γ -rays is similar to the inelastic Rayleigh scattering of x-rays in crystals. The x-ray beam interacts with the bound atoms by Compton scattering, elastic and inelastic Rayleigh scattering. In Compton scattering, the photons and loosely bound electrons interact. The electron is removed from the atom by its recoil energy and the photon is shifted to a lower energy. The Rayleigh scattering is caused by incoming x-rays which are absorbed by bound electrons which are virtually excited to a higher energy state. A photon of the same energy is re-emitted when the electron decays to its original state. The inelastically and elastically scattered photons transfer the entire recoil momentum to the lattice. The inelastic scattering also exchanges energy with the lattice by generating or absorbing a phonon. The Mössbauer 14.4keV γ -rays interact in the same way with the lattice. The main difference between the x-rays and the Mössbauer γ -rays is the width of the emission line: 1 eV for the x-rays and 5×10^{-9} eV for the zero-phonon γ -rays. The resonant scattering of γ -

rays correspond to the elastic Rayleigh scattering of photons, while the thermal diffuse scattering corresponds to the inelastic Rayleigh scattering. Both the x-rays and γ -rays will be Compton scattered. We assumed that the activity was concentrated near the surface in a thin layer. This assumption was based on observation of the relative intensities of the 14.4keV radiation, Fe x-rays, and the fluorescent x-rays of the host, see figure 4. In the worst case, which was Pd, the scattering cross sections were such that the correction was less than 0.1%. The corrections for Pt and Cu were a factor of three lower, so C_c was ignored.

$1-C_w$: is the correction for Compton scattering in the beryllium radiation windows. This is also a geometry correction which was determined for the cryostat and the furnace, and it ranged up to 4%. Since the effective solid angle subtended by a window is very difficult to calculate, and since it also depends on Compton cross-section estimates, we decided to determine this correction experimentally.

Many f-measurements were made at room temperature over a period of time in all three configurations. Careful measurements were made with all three sources in the no window geometry, $C_w=1$. Then by comparing these f-measurements with those made at room temperature in the furnace and cryostat, we found empirical values for C_w for each geometry which were independent of the sources used. Using these correction factors, the room temperature f values were found to be internally consis-

tent within the statistical accuracy of the measurements, which were better than 0.5%. These empirical corrections were then used in evaluating the data at all temperatures.

We also investigated the possibility of self-absorption in the source. Self-absorption occurs when there is resonant absorption in the source, since stable Fe^{57} can be present from previous decays. The source intensity was measured, without an absorber, with and without a 9 kOe magnetic field perpendicular to the direction of measured radiation. The resulting hyperfine splitting of the emission and absorption line would result in less self-absorption and thus in a higher count rate with the applied field, if resonant self-absorption were appreciable. The two count rates agreed within 0.01% which was well within statistical accuracy.

An additional 1% correction was made to the Pt source due to the unresolved L x-ray.

IV. Data Presentation and Analysis

Our line shape measurements were made with a thin, natural iron absorber. Thin means, in this case, that the non-resonant electronic absorption and the resonant absorption were small, $\approx 5\%$ for the resonant absorption. A large electronic absorption would decrease the transmitted intensity, resulting in longer measurements. As the resonant absorption becomes larger, multiple resonant absorptions will occur in the absorber causing a broadening of the line width. The three sources showed lines of Lorentzian shape with full width at half maximum of: Cu 0.20 .01 mm/sec, Pt 0.21 .01 mm/sec, and Pd 0.21 .01 mm/sec. Using a thin natural iron absorber, the natural line width is 0.20 mm/sec.

The data from our f -measurements are plotted as a function of temperature for Pt, Pd and Cu in figures 10, 11 and 12. In addition to our data, other investigators' data have been plotted^{3,4,5,6,7,8}.

We found an excellent fit to our data using the Debye curve corrected for anharmonicity, equation 38, as is shown by the solid line in the figures. The Debye curves were fit to the data by choosing an ϵ and calculating the corresponding θ_D for each data point above 150°K. ϵ was then varied until the values of the Debye θ showed a minimum standard deviation. The final values of θ_D and ϵ are shown on the graphs.

Because of equipartition of energy at high temperature (in our case $\geq 150^\circ\text{K}$), either a θ_D or θ_E could be found to give a good fit to our data in this temperature region. In an attempt to identify which approximation gave the best fit, the low temperature data for Pt and Pd were plotted against T^2 in figures 13 and 14. The T^2 plot was prompted by the low temperature expansion of the $-\ln f_D$, equation 26, which showed $-\ln f$

proportional to T^2 . Superimposed on the data is equation 26 for two θ_D 's, the solid curves, and equation 44 for the Einstein model, the dashed curve. Our interpretation of these graphs is that Fe^{57} in Pd behaves like a Debye solid until magnetic splitting occurs, while Fe^{57} in Pt shows possible low temperature deviation from pure Debye behavior which might be interpreted as a mixture of Debye and Einstein behavior.

In figures 10 and 11 both Pt and Pd show a decrease in f at low temperatures, below that predicted by any harmonic lattice model. Both materials are known to show magnetic splitting when alloyed with dilute iron, the larger the concentration of iron in the alloy the higher the magnetic transition temperature. This magnetic hyperfine structure would cause part of the zero-phonon γ -rays to fall outside of the absorption line of the wide absorber, thereby fortuitously lowering the measured value of f . To determine whether magnetic splitting had caused the low temperature decrease in f , both samples were rediffused for approximately four hours. After rediffusion both sources showed large increases in high energy background and x-ray radiation relative to the 14.4keV intensity, indicating the activity had been put much deeper into the host material, which reduced the local concentration of Fe at the surface. The f was again measured down to approximately 4°K and this time no anomalous decrease in f was detected, which indicated a lowering of the magnetic transition temperature. The new f measurements were not used, however, because the higher background and lower overall intensities reduced the accuracy by a factor of two or three compared to the original measurements.

If the Debye $\langle x^2 \rangle$ calculations really held for the crystal, one θ_D would characterize the complete temperature range. Experimentally, at

least two θ_D 's can be fit to the data, one at low temperatures and another above 150°K. This means that the real $D(\omega)$ deviates from the Debye model.

We would like to find out something of the real crystal frequency spectrum. Putting equation 11 into an equivalent form¹:

$$48) \quad \langle x^2 \rangle = \frac{\hbar^2}{NM} \int_0^{\omega_m} \coth\left(\frac{\hbar\omega}{2kT}\right) \frac{D(\omega)}{\omega} d\omega$$

At high temperatures, $\hbar\omega_m/kT < 2\pi$, $\coth(\hbar\omega/2kT)$ in equation 48 can be expanded to yield:

$$49) \quad \langle x^2 \rangle = \frac{kT}{M} \int_0^{\omega_m} \left[1 + \frac{1}{12} \left(\frac{\hbar\omega}{kT} \right)^2 - \frac{1}{720} \left(\frac{\hbar\omega}{kT} \right)^4 + \dots \right] \frac{D(\omega)}{\omega} d\omega$$

If we use the moments of the frequency spectrum defined as:

$$50) \quad \overline{\omega^n} = \int_0^{\omega_m} D(\omega) \omega^n d\omega$$

the low temperature limit becomes:

$$51) \quad \langle x^2 \rangle_{T=0} = \frac{\hbar}{2M} \overline{\omega^{-1}}$$

and the high temperature limit becomes:

$$52) \quad \langle x^2 \rangle_T = \frac{k}{M} \left[\overline{\omega^2} T + \frac{1}{12} \left(\frac{\hbar}{k} \right)^2 T^{-1} - \frac{1}{720} \left(\frac{\hbar}{k} \right)^4 \overline{\omega^2} T^{-3} + \dots \right]$$

For each moment $\overline{\omega^n}$, a weighted Debye θ can be defined; which becomes simply a weighted parameter of the measurements:

$$53) \quad \theta_D(n) = \frac{\hbar}{k} \left[\frac{n+3}{9N} \overline{\omega^n} \right]^{\frac{1}{n}} \quad n > -3$$

From equation 51, the low temperature expansion of $\langle x^2 \rangle$, one can extract a weighted $\theta_D(-1)$. From equation 52 a series of characteristic thetas are

theoretically available. Our accuracy, however, was such that we were only able to obtain $\theta_D(-2)$ from the high temperature expansion.

Lipkin²⁰ has shown that an impurity that goes into a harmonic host with no change in force constants will result in the $\theta_D(-1)$ relation:

$$54) \quad \theta_D(-1)_{\text{eff}} = \left[\frac{M'}{M} \right]^{-1/2} \theta_D(-1)_{\text{host}}$$

within a few percent. Any substantial deviation from equation 54, then, would show a change in the force constants of the impurity-host compared to the host-host. Table I lists the $\theta_D(-1)_{\text{host}}$ calculated by various investigators, the $\theta_D(-1)_{\text{imp}}$ we calculated from our data, and the mass ratio of impurity to host, M'/M . Line four of the table shows the ratio of $\theta_D(-1)_{\text{imp}}/\theta_D(-1)_{\text{eff}}$; a ratio of one indicating no change in force constants. From these data we conclude that Fe^{57} in Cu has larger force constants than Cu in Cu, while the force constants for Fe^{57} in Pt and Pd are smaller than those for the host atoms.

The anharmonicity parameter, ϵ , for the impurity in the host and for the pure host are given in the last two lines of Table I. From these figures we conclude that the Fe^{57} in Cu is much more anharmonic than the host material, while Fe^{57} in Pt and Pd show about the same anharmonicity as the host.

A complete tabulation of the experimental data as well as a more detailed discussion of the results is given in a paper by Nussbaum, Howard, Nees, and Steen²³.

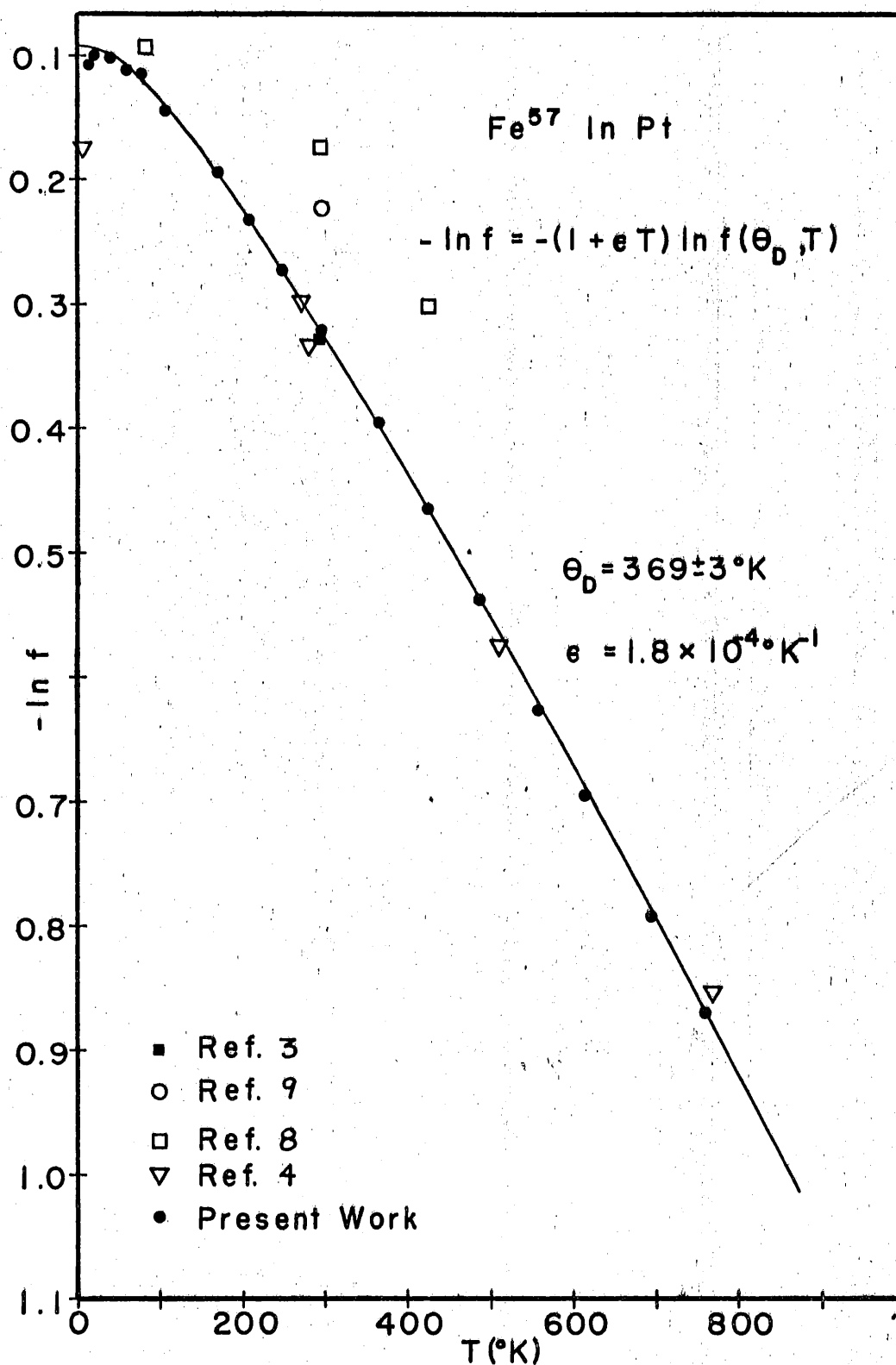


Figure 10. The recoil free fraction of Fe^{57} in a single crystal of Pt.

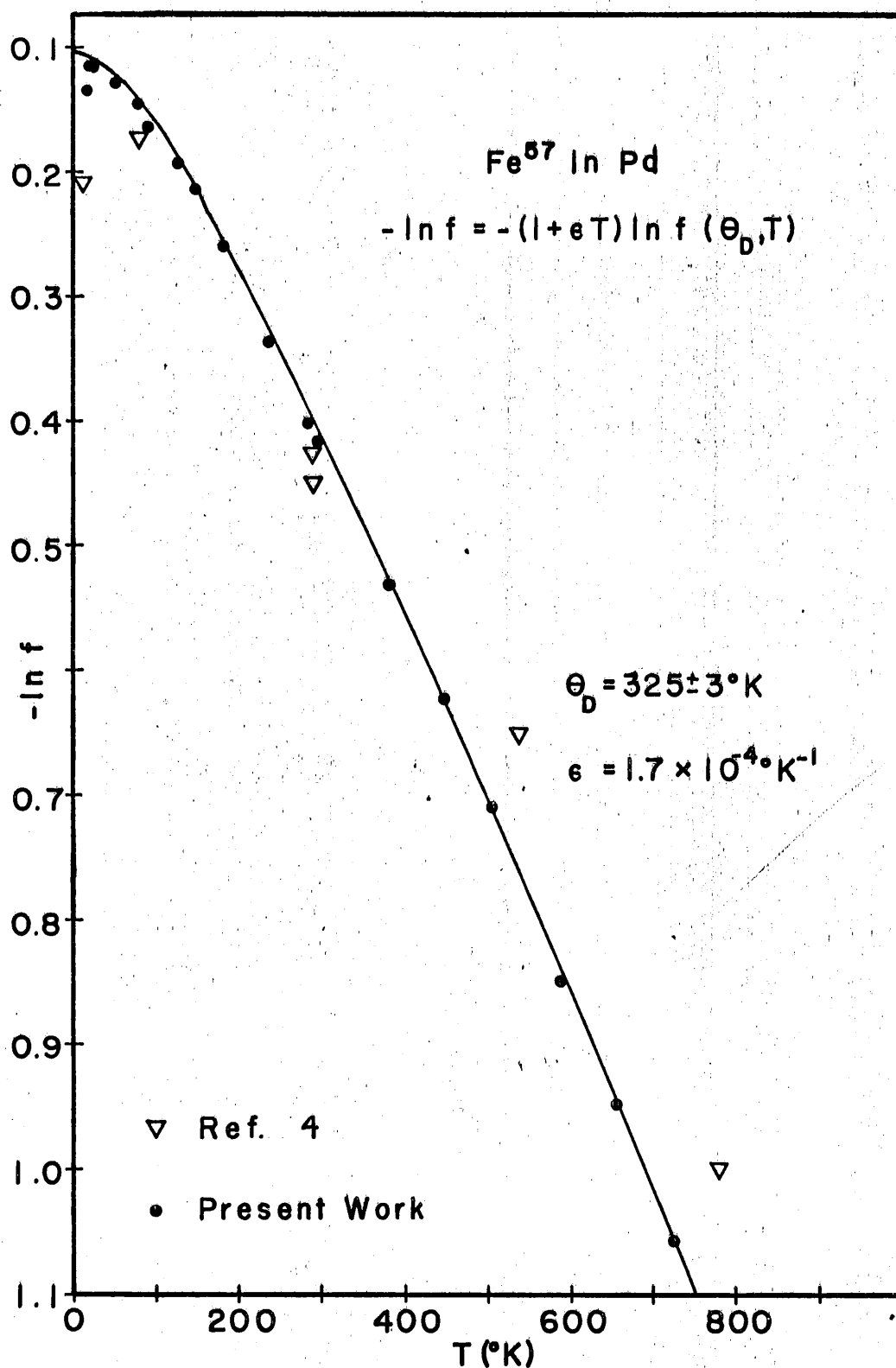


Figure 11. The recoil free fraction of Fe^{57} in single crystal Pd.

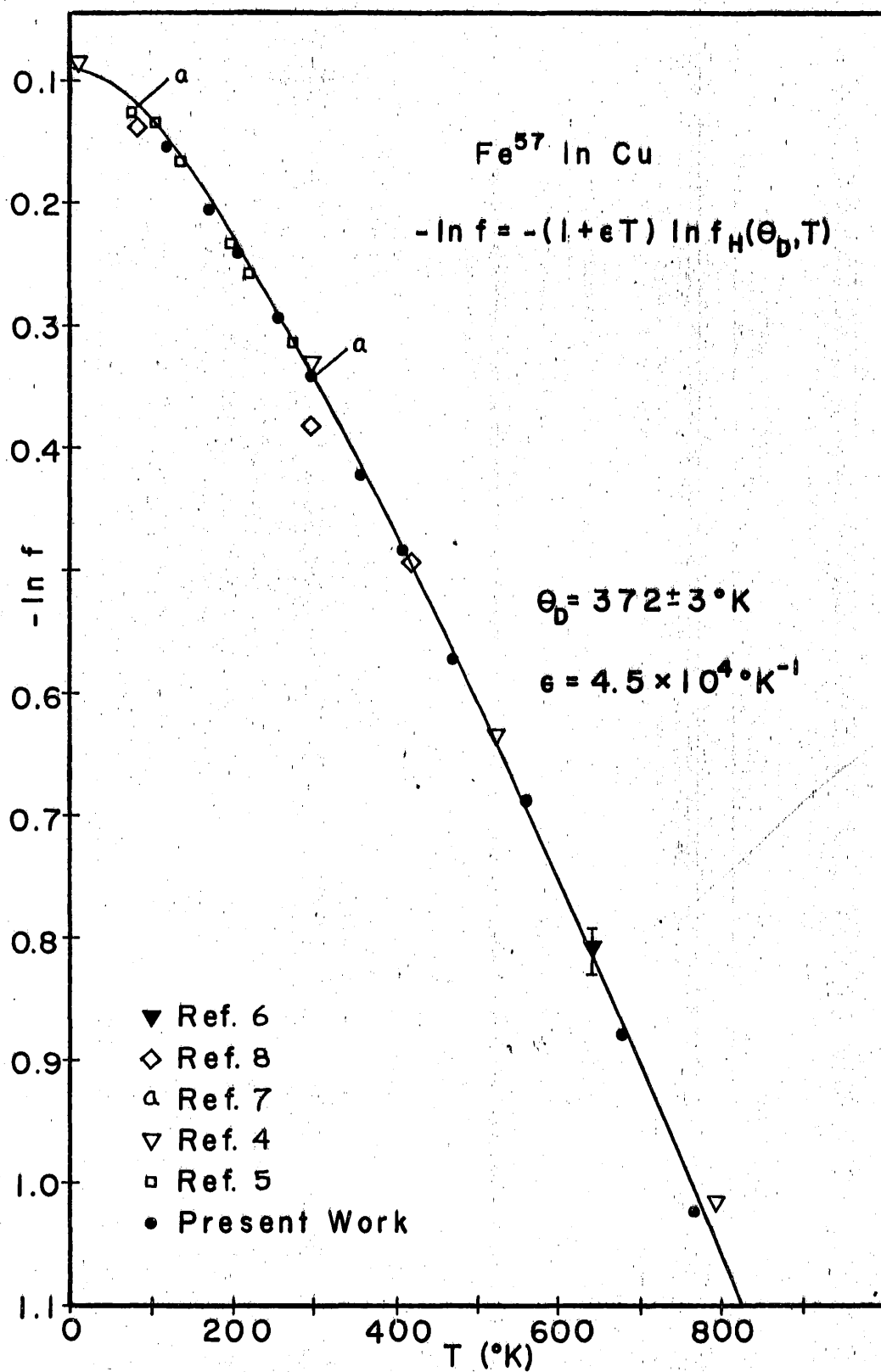
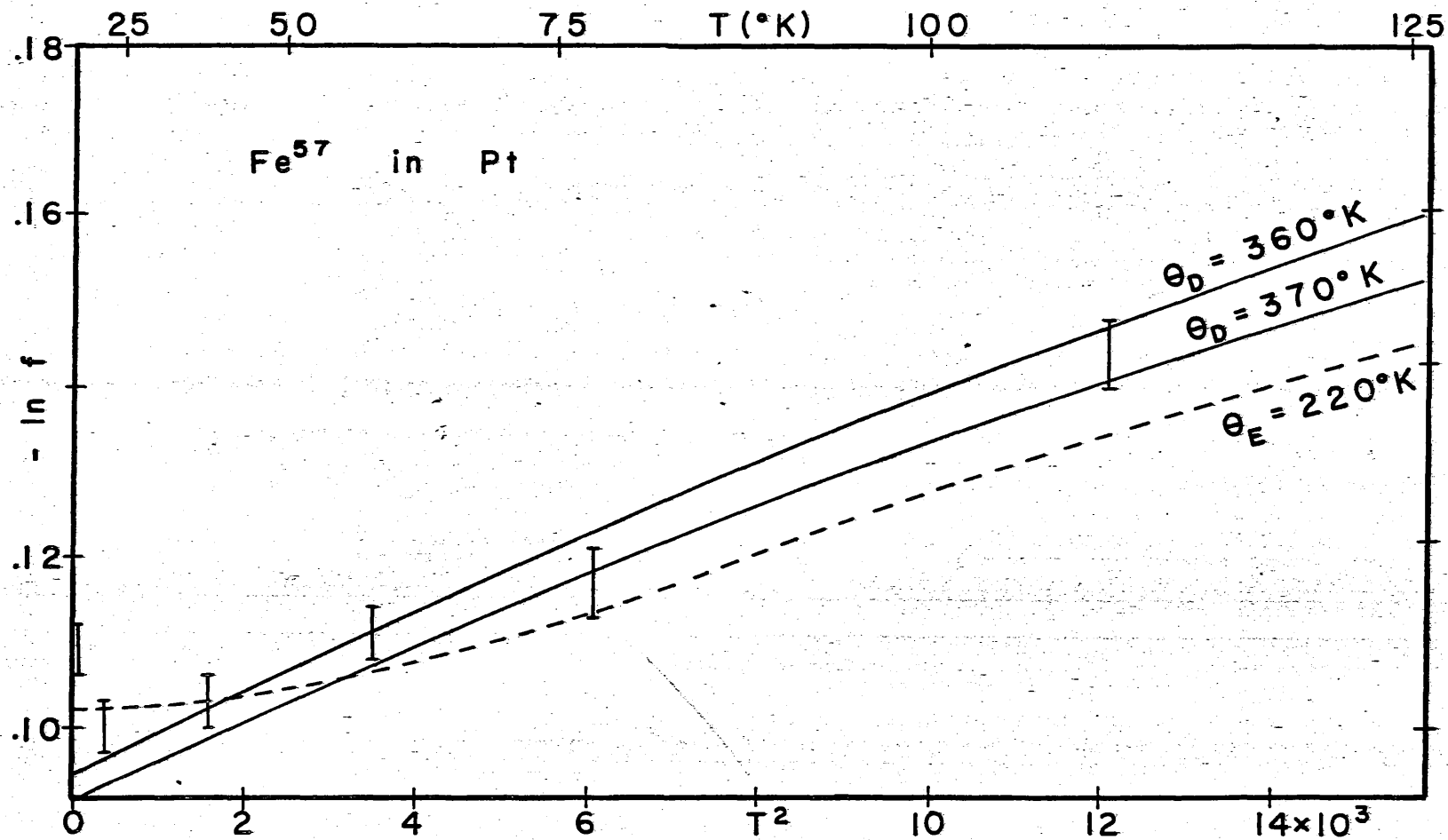


Figure 12. The recoil free fraction of Fe^{57} in single crystal Cu.

Figure 13. The low temperature Pt data versus T^2 , for explanation see text.



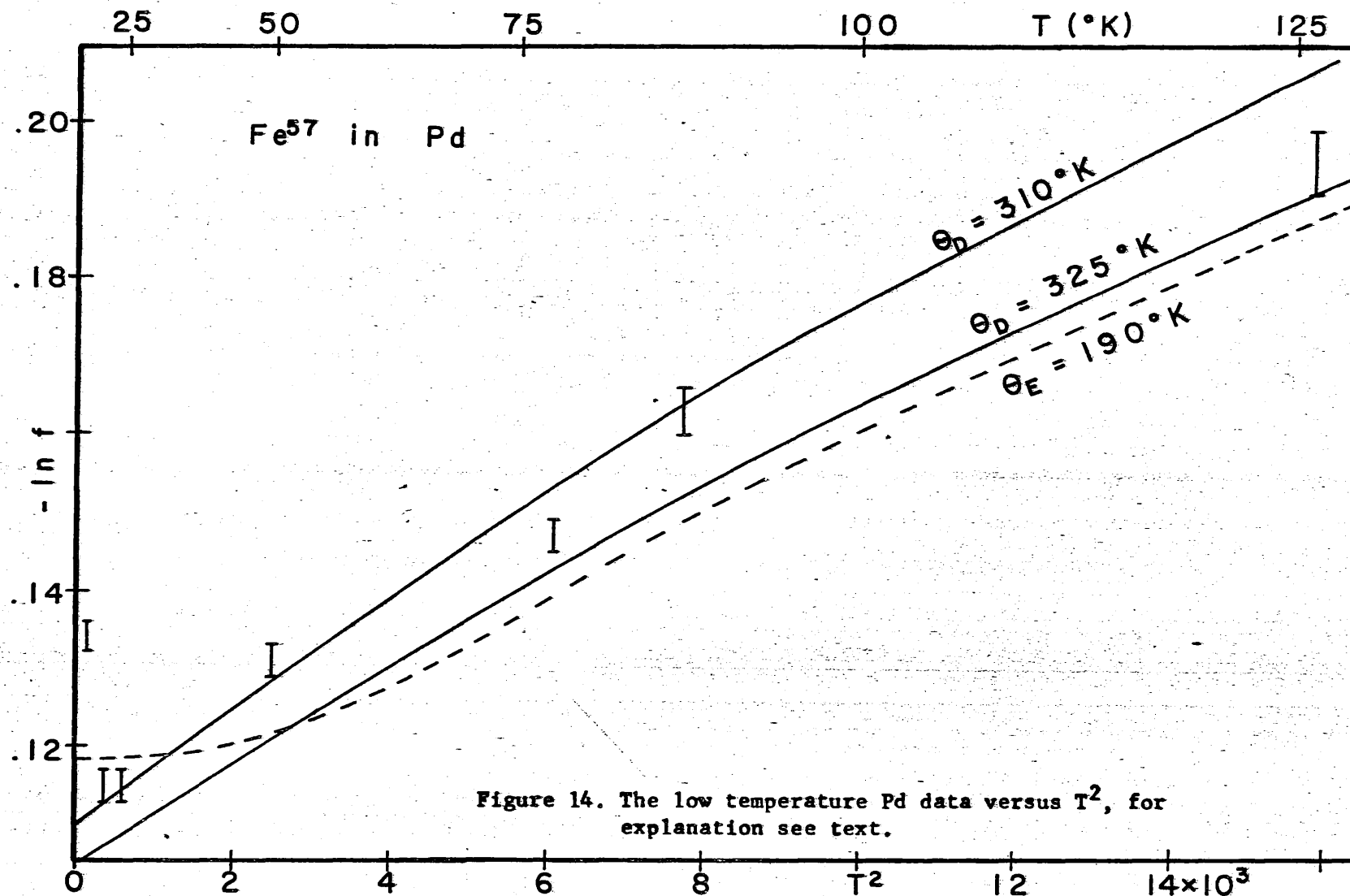


Table I. Summary of Data.

	Pt	Pd	Cu
$\theta_D(-1)_h$	231° (a)	249° (b)	326° (c)
$\theta_D(-1)_i$	360 \pm 10°	310 \pm 10°	363 \pm 7°
M^*/M	0.29	0.54	0.90
$\frac{\theta_D \text{ imp}}{\theta_D \text{ eff}}$	0.84	0.92	1.06
$\epsilon \text{ imp} \times 10^4$	1.8 \pm 0.3	1.7 \pm 0.3	4.5 \pm 0.5
$\epsilon \text{ host} \times 10^4$	1.3 (c)	1.6 (d)	1.8 (d)

(a) Ref. 21

(c) Ref. 13

(b) Ref. 22

(d) Thermodynamic Data

V. Bibliography

1. G. K. Wertheim, "Mössbauer Effect" (Academic Press, NY, 1963).
2. H. Frauenfelder, "The Mössbauer Effect", (W. A. Benjamin, NY, 1963).
3. R. M. Housely, N. E. Erickson, and J. G. Dash, Nucl. Instr. and Methods, 27, 29 (1964).
4. W. A. Steyert and R. D. Taylor, Phys. Rev. 134, A716 (1964).
5. D. L. Sprague, Thesis, University of Washington, Seattle (1967).
6. D. G. Howard and J. G. Dash, J. Appl. Phys. 38, 991 (1967).
7. R. M. Housely, J. G. Dash, and R. H. Nussbaum, Phys. Rev. 136, A464 (1964).
8. J. P. Schiffer, P. N. Parks, and J. Heberle, Phys. Rev. 133, A1553 (1964).
9. W. Kerler and W. Neuwirth, Z. Physik 167, 194 (1962).
10. A. J. F. Boyle and H. E. Hall, Rept. Progr. Phys. 25, 441 (1962).
11. C. Kittel, "Introduction to Solid State Physics" (J. Wiley & Sons, NY, 1966).
12. W. M. Visscher, Phys. Rev., 129, 1 (1963).
13. R. M. Nicklow, G. Gilat, H. G. Smith, L. S. Raubenheimer and M. K. Wilkinson, Phys. Rev. 164, 922 (1967).
14. A. H. Muir, "Tables and Graphs for Computing Debye-Waller Factors in Mössbauer Effect Studies", Atomic International Doc. AI-6699 (1962).
15. A. A. Maradudin and P. F. Flinn, Phys. Rev. 129, 2529 (1963).
16. W. Heitler, The Quantum Theory of Radiation, Oxford University Press, (1944).
17. Nuclear Spectroscopy, Academic Press, NY (1960), p. 218.
18. This absorber was loaned to us by R. D. Taylor at Los Alamos Scientific Laboratory.
19. R. M. Housely, Nucl. Instr. and Methods 35, 77 (1965).
20. H. J. Lipkin, Ann. Phys. (NY) 23, 28 (1963).
21. J. L. Feldman and G. K. Horton, Phys. Rev. 137, A1106 (1965).

22. B. W. Veal and J. A. Rayne, Phys. Rev. 135, A442 (1964).
23. R. H. Nussbaum, D. G. Howard, W. L. Nees and C. F. Steen, "Lattice Dynamical Properties of Fe⁵⁷ Impurity Atoms in Pt, Pd, and Cu From Precision Measurements of Mössbauer Fractions", (to be published).